NASA Contractor Report 189681
ICASE Report No. 92–31

ICASE

ON THE SPATIAL EVOLUTION OF LONG-WAVELENGTH GÖRTLER VORTICES GOVERNED BY A VISCOUS-INVISCID INTERACTION

PART 1: THE LINEAR CASE

Meelan Choudhari
Philip Hall
Craig Streett

Contract No. NAS1–18605
July 1992

Institute for Computer Applications in Science and Engineering
NASA Langley Research Center
Hampton, Virginia 23665–5225

Operated by the Universities Space Research Association

National Aeronautics and
Space Administration

Langley Research Center
Hampton, Virginia 23665-5225

ON THE SPATIAL EVOLUTION OF LONG-WAVELENGTH GÖRTLER VORTICES GOVERNED BY A VISCOUS-INVISCID INTERACTION PART 1: THE LINEAR CASE

Meelan Choudhari
High Technology Corporation
Hampton, VA 23666

Philip Hall[1]
University of Manchester
Manchester, M13 9PL, UK

Craig Streett
NASA Langley Research Center
Hampton, VA 23665

ABSTRACT

The generation of long-wavelength, viscous-inviscid interactive Görtler vortices is studied in the linear regime by numerically solving the time-dependent governing equations. It is found that time dependent surface deformations, which assume a fixed nonzero shape at large times, generate steady Görtler vortices that amplify in the downstream direction. Thus, the Görtler instability in this regime is shown to be convective in nature, contrary to the earlier findings of Ruban and Savenkov. The disturbance pattern created by steady and streamwise-elongated surface obstacles on a concave surface is examined in detail, and also contrasted with the flow pattern due to roughness elements with aspect ratio of order unity on flat surfaces. Finally, the applicability of the Briggs-Bers criterion to unstable physical systems of this type is questioned by providing a counterexample in the form of the inviscid limit of interactive Görtler vortices.

[1]This research was supported by the National Aeronautics and Space Administration under NASA Contract No. NAS1-18605 while the author was in residence at the Institute for Computer Applications in Science and Engineering, NASA Langley Research Center, Hampton, VA 23665.

1 Introduction

The physical realizability of an unstable equilibrium solution corresponding to a nearly homogeneous shear flow is dependent on whether or not the equilibrium state corresponds to the time-asymptotic solution of the related unsteady problem. The answer to this latter question can usually be obtained quite easily, provided one has sufficient information to classify the linear instabilities of this equilibrium state as being of either absolute or convective nature (Briggs 1964, Bers 1975, Huerre and Monkewitz, 1985). The presence of an absolute instability means that any compact unsteady source with a continuous Fourier spectrum will introduce disturbances that amplify indefinitely in time at all neighbouring locations, thereby eliminating the possibility of any time-asymptotic state within the linear framework. In contrast, the response of a convectively unstable flow to a pulsed source takes the form of an instability-wave packet that is swept away from the source by the mean flow, thus restoring the original state at sufficiently large times.

For convectively unstable flows, it is also possible to investigate the response of the flow to some continuous forcing in a local region, say in the form of a time-harmonic disturbance which is switched on at a finite time. The time-asymptotic solution to a "signalling" problem of this type can be obtained either from a superposition of the wave-packet solutions Balsa (1988), or by directly solving the steady state equations which have the harmonic time dependence built into them. The overall amount of effort required is perhaps larger in the former case; however, it automatically ensures the causality of the steady-state response, without any need (as in the latter case) for extraneous considerations such as the Briggs-Bers criterion in order to specify the correct streamwise boundary conditions at the upstream and/or downstream ends.

The objective in this paper is to consider the above issues in the context of a centrifugal, i.e., the Görtler instability of boundary-layer flows over concave surfaces. Experiments have shown that this instability is usually manifested in the form of steady streamwise vortices which amplify in the downstream direction, eventually yielding to time-dependent instabilities of a secondary and tertiary nature. The various experimentally observed features of the linear and nonlinear development of the Görtler vortices have also been explained using asymptotic theories (Hall 1982a-b, Hall and Lakin 1988, Hall 1990), and direct numerical simulations (Hall 1988, Sabry and Liu 1990, Liu and Sabry 1991).

While the occurence of steady unstable vortices is suggestive of a convective nature for the Görtler instability, the validity of this assumption had not been addressed until Parks and Huerre (1988), who examined the special case of an asymptotic suction profile. More recently, Ruban (1990) (herafter referred to as R) examined the Görtler instability of an arbitrary profile in the long-wavelength regime using asymptotic methods in the limit of a large Reynolds number R, and a large Görtler number G. Somewhat surprisingly, he found that the flow is absolutely unstable to spanwise-periodic perturbations. However, he also examined the disturbances created by an isolated point source and concluded that the flow is convectively unstable in this latter case. Here, the wave packet, determined through steepest-descent analysis, was found to spread in all directions including upstream, except for a sector of 60^0 directly ahead of the source.

Savenkov (1990) (henceforth, S) applied the same asymptotic framework as Ruban to study the receptivity problem for the Görtler vortices in the long-wavelength regime. He used a residue analysis in conjunction with Fourier transform methods to compute the approximate temporal development of the perturbations created by an unsteady wall hump which assumes its final

(nonzero) shape after a finite length of time. His results were supportive of the conclusions in R, in that the steady-state pattern was found to be similar in shape to the time-dependent wave packet of R, and no Görtler vortices were generated downstream of the hump. Previously, Rozhko *et al* (1988) (henceforth, RRT) had also studied the same problem, albeit by solving the steady state equations directly in Fourier transform space. The disturbance pattern computed in this manner was also similar to that obtained by S as a limit of the time-dependent problem. RRT had also found that a crucial difference between the disturbance patterns on concave and convex walls corresponds to the presence of an $O(1)$ upstream signature in the former case, as against a total lack of any upstream influence in the latter case.

The above results concerning the absolute nature of the Görtler instability, as well as the occurence of an upstream interaction in the concave-wall case, are rather intriguing, the former, since it casts a doubt on the relevance of much of the previous work on Görtler instability which was related to steady vortices, and the latter, due to the fact that the steady-state equations are actually parabolic in nature. In this paper we examine the problems addressed by R, S and RRT, and demonstrate that the peculiar findings of these investigators are actually a result of having ignored a fundamental property of the partial differential equations governing the steady and unsteady problems. Specifically, we show that solving the unsteady problem with the appropriate boundary conditions not only confirms the convective nature of Görtler instability in the spanwise-periodic case, but also yields the solution to the receptivity problem in the limit of large times.

The problem of the generation and subsequent linear development of long-wavelength Görtler vortices is formulated in the following section. Although no extra effort is involved in solving the complete problem related to viscous-inviscid interactive vortices, it is more illustrative to separately consider the two limiting cases corresponding to the viscous and inviscid vortices, respectively. Both analytical and numerical methods are used towards this purpose; the analytical work is presented in Section 2, whilst in Section 3 we present our results. Finally we draw some conclusions in Section 4.

2 The governing equations for viscous-inviscid interactive longitudinal vortex structures and some analytical results

At a given value of the curvature parameter, *viz.* the Görtler number $G = \frac{L^*}{a^*} Re_{L^*}^{1/2}$, the linear development of steady Görtler vortices is determined primarily by the nondimensional wavelength in the spanwise direction, $\lambda_z = Re_{L^*}^{1/2} \frac{\lambda_z^*}{L^*}$. Here L^* denotes a typical streamwise length scale based on the distance between the leading edge and the location of interest, a^* ($>> O(L^*)$) is the radius of curvature of the surface at this location, and $Re_{L^*}(>> 1)$ is the Reynolds number based on the local free-stream speed U_∞^*, and the distance L^*. The asterisk is used to indicate the dimensional quantities here, and throughout the rest of this paper.

It was shown independently by Denier, Hall and Seddougui (1990), and Timoshin (1990) that in the limit of large Görtler numbers ($G >> 1$) one needs to consider five different asymptotic regimes along the λ_z axis. In the order of increasing spanwise wavelength, these regimes correspond to (i) the neutral regime ($\lambda_z \sim G^{-1/4}$), (ii) the most unstable regime ($\lambda_z \sim G^{-1/5}$),

(iii) the inviscid regime ($\lambda_z = O(1)$), (iv) the long wavelength or viscous-inviscid interactive regime ($\lambda_z \sim G^{1/7}$), and finally, (v) the nonparallel regime corresponding to $\lambda_z = O(G^{1/2})$. Investigations of the linear and nonlinear stability problems associated with the first three of these five regimes have been given by Hall (1982a-b), Hall and Lakin (1988), Denier, Hall and Seddougui (1990), and Timoshin (1990). The viscous-inviscid regime for Görtler vortices was first investigated by Rozhko and Ruban (1987) in connection with the disturbances generated by streamwise-elongated roughness elements over curved surfaces, and subsequently, in the same context by RRT, R and S, as mentioned already. The fifth regime corresponding to nonparallel vortices does not appear to have been studied in any detail until now, but see Hall(1983).

As stated in the Introduction, our concern in this paper is with the generation and linear amplification of the long wavelength, or viscous-inviscid interactive Görtler vortices, which are relevant at locations close to the leading edge. As first shown by RR, the asymptotic scalings of this regime are fixed by the condition of viscous-inviscid interaction, plus a balance of the displacement-induced pressure with the jump in pressure across the main part of the boundary layer due to centrifugal effects associated with the surface curvature. These balances identify the spanwise length scale λ_z, based on the boundary-layer thickness, as being of $O(\epsilon^{-1})$, where $\epsilon = G^{-1/7}$ ($<< 1$), whereas the streamwise length scale ℓ_x, based on the distance L^* from the leading edge, is determined to be $O(\epsilon^3)$. In the normal direction, the vortex structure consists of three distinct subregions, *viz.* the lower, middle and upper decks, whose thicknesses relative to that of the boundary layer are of $O(\epsilon), O(1)$, and $O(\epsilon^{-1})$ respectively. The overall dynamics of each of the decks, as well as their coupling, is quite analogous to that in the conventional three-dimensional triple deck problem. The structural similarities between the two problems lead one to anticipate that the Görtler vortex problem is also amenable to the same solution procedure as that applied in triple-deck problems, and indeed, this was shown to be the case by RR. Specifically, it is possible to obtain closed form solutions for the perturbations in the middle and upper decks, and a matching of these two provides the interactive relationship between the pressure and displacement-thickness perturbation, this closes the lower-deck problem governed by some form of the three-dimensional boundary layer equations.

For the sake of definiteness, consider the same problem as that studied by both R and S, *viz.*, the disturbance pattern produced by an unsteady wall-hump with an arbitrary but specified shape that can be expressed as the coordinate surface

$$Y = 0, \tag{2.1}$$

corresponding to the Prandtl-transposed coordinate within the lower deck, $Y = \epsilon^{-1} Re_{L^*}^{1/2} \lambda^{4/7} y^*/L^* - h\,F(X,Z,T)$, where $X = \epsilon^{-3}\lambda^{5/7} x^*/L^*$ and $Z = \epsilon Re_{L^*}^{1/2}\lambda^{10/7} z^*/L^*$ are local coordinates in the streamwise and spanwise directions respectively, $T = \epsilon^2 Re_{L^*}^{1/2}\lambda^{-8/7} U_\infty^* t^*/L^*$ is the nondimensional time, and h ($<< 1$) and $F(X,Z,T)$ are, respectively, the normalized height parameter and shape function characterizing the wall-hump geometry (see Fig. 1). For reasons which will be obvious later, it is appropriate to only consider the type of hump geometries which have a definite streamwise origin, i.e., $F(X,Z,T) \equiv 0$ for X less than some finite value X_0, which will be assumed to be the origin, $X = 0$, without any loss of generality. The parameter λ is used to denote the wall shear corresponding to the incoming boundary-layer profile just upstream of the roughness element.

Introducing the expansions $(\frac{u^*}{U_\infty^*},\ \frac{v^*}{U_\infty^*},\ \frac{w^*}{U_\infty^*},\ \frac{p^*-p_{-\infty}^*}{\rho^* U_\infty^{*\,2}}) = (Y + \epsilon h \lambda^{-3/7} U,\ \epsilon^{-1} Re_{L^*}^{-1/2} h \lambda^{-4/7}(F_T +$

$YF_X + V)$, $\epsilon^{-3}Re_{L^*}^{-1/2}h\lambda^{2/7}W$, $\epsilon^{-6}Re_{L^*}^{-1}h\lambda^{4/7}P)$ for the lower deck variables, one finds that the leading-order perturbations (U, V, W, P) are governed by the linearized, three-dimensional boundary-layer equations

$$\partial_X U + \partial_Y V + \partial_Z W = 0, \tag{2.2a}$$

$$(\partial_T + Y\,\partial_X)U + V = \partial_Y^2 U, \tag{2.2b}$$

and

$$(\partial_T + Y\,\partial_X)W = -\partial_Z P + \partial_Y^2 W, \tag{2.2c}$$

without any pressure gradient along the streamwise direction. Since the surface deformation due to the unsteady hump has been assumed to originate at a finite time, the disturbance field may be taken to be zero at the initial instant of time. Similarly, it can be assumed that the surface obstacle will not produce any disturbances sufficiently far upstream, and also that the disturbance motion either decays, or remains bounded, as $|Z| \to \infty$, depending on whether $F(X, Z, T)$ has a compact or noncompact support in the spanwise direction. The boundary conditions in the normal direction are given by

$$U = V = W = 0 \ \text{ at } Y = 0, \tag{2.3a - c}$$

and

$$U \to F(X, Z, T) - A(X, Z, T), \ \ W \to 0 \ \text{ as } Y \to \infty, \tag{2.3d, e}$$

where the displacement-thickness perturbation $A(X, Z, T)$ is related to the pressure perturbation $P(X, Z, T)$ via the interactive relationship (RR)

$$\partial_Z P = -sign(G)\partial_Z A + \frac{1}{\pi}\int_{-\infty}^{+\infty} \frac{\partial_X^2 A(X, \xi)}{\xi - Z} d\xi, \tag{2.3f}$$

which reflects the simultaneous balance between the lower-deck pressure, the curvature-induced pressure within the middle deck and the displacement-induced pressure inside the upper deck. In (2.3f), the sign of the Görtler number has been assumed to be positive for concave surfaces, and negative for convex ones. Moreover, one may also obtain results for the case of an underlying surface that is flat, or has an asymptotically small curvature, by setting $sign(G) = 0$ in (2.3f). In that case, the small parameter ϵ is to be interpreted as a measure of the aspect ratio of the planform of the surface obstacle.

It is worth mentioning that apart from the absence of a streamwise pressure gradient term in equations (2.2a-c), which follows as a consequence of the length-scale disparity in the streamwise and spanwise directions, the problem of viscous-inviscid interactive vortices differs from the three-dimensional triple-deck problem in two other aspects which are related to properties of the middle and upper decks, and thus, are manifested through the interactive relationship (2.3f). Firstly, the role of the main deck is no longer just a passive one, corresponding to a direct transmission of the outer pressure to the lower deck, since the centrifugal effects in the middle deck now substantially alter the pressure gradient imposed on the lower deck. As seen from equation (2.3f), the pressure jump across the middle deck turns out to be independent of the details of the incoming boundary-layer profile, being equal to just the normalized displacement-thickness A in terms of its magnitude. For this reason, the equation set (2.2-2.3) is a canonical one and, indeed, after some additional analysis, it can be shown to be valid at both subsonic and

supersonic speeds. The other source of differences between the Görtler-vortex and triple-deck problems is related to the behaviour in the upper deck where, due to the negligible pressure gradient in the streamwise direction, the secondary flow in the cross-flow plane is decoupled from the local streamwise motion, in a manner somewhat analogous to slender body theory. As a result, the upper deck motion is elliptic only within the cross-flow $(Y - Z)$ plane and, thus, cannot exert an $O(1)$ upstream influence on the lower deck motion *via* the pressure-displacement relation (2.3f).

Applying a Fourier transform in the spanwise direction $(Z \rightarrow k)$, and denoting the transformed variables using an overbar, the governing equations can be rewritten as

$$\partial_X \bar{U} + \partial_Y \bar{V} + ik\bar{W} = 0, \tag{2.4a}$$

$$(\partial_T + Y\,\partial_X)\bar{U} + \bar{V} = \partial_Y^2 \bar{U}, \tag{2.4b}$$

and

$$(\partial_T + Y\,\partial_X)\bar{W} = -ik\bar{P} + \partial_Y^2 \bar{W}, \tag{2.4c}$$

along with the boundary conditions

$$\bar{U} = \bar{V} = \bar{W} = 0 \text{ at } Y = 0, \tag{2.5a-c}$$

$$\bar{U} = \bar{F}(X,Z,T) - \bar{A}(X,Z,T), \;\; \bar{W} = 0 \text{ as } Y \rightarrow \infty, \tag{2.5d,e}$$

and

$$k\bar{P} = -sign(G)k\bar{A} + sign(k)\,\bar{A}_{XX}, \tag{2.5f}$$

obtained from (2.3a-f), plus the homogeneous initial conditions in X and T.

In the following section, we present numerical solutions to the unsteady problem posed above for the case of spanwise-periodic perturbations, and confirm the lack of any absolute instability by demonstrating the appearance of an unstable, spatially-growing Görtler vortex at large times. It is also possible to obtain closed-form, analytical solutions by taking the appropriate transform along the streamwise direction. For instance, RRT, R and S used a two-sided Fourier transform in their work; but, one should note that using a Fourier transformation along the streamwise direction in unstable physical systems is not always a straightforward matter, although fairly standardized recipes, such as the Briggs-Bers criterion (see Briggs 1964, Bers 1975), are now available to treat this issue in the case of streamwise elliptic systems. Now, due to a lack of the streamwise pressure gradient as well as streamwise diffusion terms, the system (2.2-2.3) is not elliptic in X and Y. In fact, in the limit of very long wavelength vortices, it can be easily shown to be parabolic in the streamwise direction; refer to the discussion following Eq. (2.12d). Noting the failure of RRT, R, and S in accounting for this anticipated lack of upstream influence in the concave-wall case, it would seem that a straightforward application of the Fourier transform technique in non-elliptic unstable systems may lead to physically unacceptable results; In Section 3.1 below, we will also consider the short-wavelength (or inviscid) limit of the problem, and illustrate the inapplicability of Briggs-Bers criterion towards predicting the nature of instability in that case.

Thus, consider the Laplace transform solution to the problem posed by equations(2.4-2.5), which is given by

$$\bar{A}(\beta,k,\sigma) = \frac{\beta^{5/3} Ai'(\zeta_0)\bar{F}(\sigma,\beta)}{\beta^{5/3} Ai'(\zeta_0) + [sign(G)\,k^2 - |k|\beta^2] \int_{\zeta_0}^{\infty} Ai(\tilde{\zeta})\,d\tilde{\zeta}}, \tag{2.6a}$$

$$k\bar{P} = [\beta^2 sign(k) - k sign(G)]\bar{A}, \tag{2.6b}$$

$$\bar{U} = \frac{-k^2\bar{P}}{\beta^{5/3}}\{\frac{\int_{\zeta_0}^{\zeta} Ai(\tilde{\zeta})\,d\tilde{\zeta}}{Ai'(\zeta_0)} + \pi[Gi(\zeta) - \frac{Gi(\zeta_0)}{Ai(\zeta_0)}Ai(\zeta)]\}, \tag{2.6c}$$

$$\bar{W} = \frac{-ik\pi\bar{P}}{\beta^{2/3}}[Gi(\zeta) - \frac{Gi(\zeta_0)}{Ai(\zeta_0)}Ai(\zeta)], \tag{2.6d}$$

and $\bar{V}$ follows from the X-momentum equation, (2.4b). Here σ and β denote the transform variables corresponding to the time T, and the streamwise coordinate X respectively, while ζ is defined as

$$\zeta = \beta^{1/3}Y + \zeta_0, \quad \zeta_0 = \frac{\sigma}{\beta^{2/3}}, \tag{2.6e,f}$$

The dispersion relationship corresponding to the Görtler vortex instability modes is then given by

$$D(\sigma,\beta;k) \equiv \frac{\beta^{5/3}Ai'(\zeta_0)}{\int_{\zeta_0}^{\infty} Ai(\tilde{\zeta})\,d\tilde{\zeta}} + sign(G)k^2 - |k|\beta^2 = 0, \tag{2.7a}$$

$$(L) \qquad (M) \qquad (U)$$

which further reduces to

$$3Ai'(0)\beta^{5/3} + sign(G)k^2 - |k|\beta^2 = 0, \tag{2.7b}$$

for the case of steady vortices ($\sigma = 0$), which are apparently more important in practice than the unsteady ones. An interesting property of the steady dispersion relation (2.7b) is that it possesses a unique root in the complex β plane for any given (real) spanwise wavenumber k, and moreover, this root always lies on the real, positive β axis, implying that the steady vortices exhibit a purely exponential growth in the streamwise direction. A plot of the stationary growth rate β as a function of the spanwise wavenumber k is shown by the solid curve in Fig. 2, where the large and small k asymptotes, given by (2.8b) and (2.9b) below, are also indicated by the two dashed curves.

As described earlier, both the unsteady as well as steady dispersion relations represent a balance between the effects of viscosity in the lower deck (L), destabilizing centrifugal forces in the middle deck (M), and the viscous-inviscid interaction via the upper deck (U). However, in the limit of large spanwise wavenumbers ($k >> 1$), and commensurably larger frequencies ($|\sigma| >> 1$), the dominant balance shifts to just the inviscid terms (M-U) in (2.7a,b) together with the large σ form of (L), and is given by

$$-\sigma\beta + sign(G)k^2 - |k|\beta^2 = 0, \tag{2.8a}$$

in the unsteady case. For the steady problem (L) is negligible and we obtain

$$sign(G)k^2 - |k|\beta^2 = 0, \tag{2.8b}$$

which matches with the dispersion relation in the main inviscid regime corresponding to stationary vortices with spanwise wavelengths comparable to the boundary-layer thickness; see Denier, Hall and Seddougui (1990), and also Timoshin (1990). In contrast, the opposite limit of extra-long spanwise wavelengths ($k << 1$), which was the focus of the work by RRT, R and S, leads to the purely noninteractive, viscous-centrifugal (L-M) balances

$$\frac{\beta^{5/3} Ai'(\zeta_0)}{\int_{\zeta_0}^{\infty} Ai(\tilde{\zeta})\, d\tilde{\zeta}} + sign(G) k^2 = 0, \tag{2.9a}$$

and

$$3Ai'(0)\beta^{5/3} + sign(G) k^2 = 0, \tag{2.9b}$$

in the unsteady and steady cases, respectively.

Finally, setting $sign(G) = 0$ in (2.7a) yields the interactive, flat-surface limit,

$$\frac{\beta^{5/3} Ai'(\zeta_0)}{\int_{\zeta_0}^{\infty} Ai(\tilde{\zeta})\, d\tilde{\zeta}} - |k|\beta^2 = 0, \tag{2.10}$$

which corresponds to very oblique Tollmien-Schlichting waves (Hall and Morris 1991), and could also have been obtained by taking the appropriate limit of the full three-dimensional triple deck equations. Since our primary interest lies in the Görtler vortex type of instabilities, the limits (2.8) and (2.9) are more relevant to us than (2.10), and therefore, we shall choose to concentrate on these two cases in the remaining part of this paper. Of particular interest will be the extra-long wavelength problem which is exemplified by the dispersion relationships (2.9a,b) and, was also considered by RRT, R, and S. For this case, it is possible to further substantiate the lack of any upstream influence in a manner described below.

Basically, further manipulation of equations (2.4) leads to a single partial differential equation for the vertical velocity perturbation,

$$[\partial_Y^2 - (\partial_T + Y\partial_X)]\partial_Y^2 \bar{V} = 0, \tag{2.11}$$

which, together with the boundary conditions

$$\bar{V} = \partial_Y \bar{V} = 0 \text{ at } Y = 0, \tag{2.12a-b}$$

$$\partial_Y^2 \bar{V}(\infty) = 0, \tag{2.12c}$$

and

$$\partial_X \partial_Y^3 \bar{V}(0) + sign(G)\, k^2 \left[\partial_Y \bar{V}(\infty) + \partial_X \bar{F}(X, Z, T)\right] = 0,, \tag{2.12d}$$

and the homogeneous initial conditions in X and T directions, can be viewed as a one parameter (*viz.* Y) family of linear advection equations in the $X - T$ space with a positive semi-definite range of convection velocities, the member equations being coupled via normal diffusion, and the integral evolutionary constraint (2.12d). The nature of these advection equations lends further support to our previous argument concerning the lack of any upstream influence in the problem. Since the propagation of disturbances in the upstream direction is prohibited, the homogeneous initial condition in the streamwise direction can be imposed just upstream of the origin of the surface nonuniformity, i.e. at $X \rightarrow 0-$. One should also note that the above classification of

the governing partial differential equations is independent of the sign, or the magnitude, of the curvature parameter G, since it only appears through the coefficient of a zeroth-order derivative term in (2.12d). The only difference between the convex and concave cases corresponds to the existence of a Görtler instability in the latter case, which leads to disturbance amplification in the downstream direction. This aspect appears to have been overlooked by RRT, R and S, who utilized a two-sided Fourier transform in the streamwise direction without accounting for the properties of the governing differential equations.

3 Numerical Results

In this section we present the numerical solutions to the set of governing equations corresponding to (2.2) and (2.3). The case of spanwise periodic perturbations is examined first in Section 3.1, followed by the case of an isolated surface excrescence, which is discussed in Section 3.2. In both cases, spectral discretizations, Chebyshev and Fourier, respectively, were utilized along the Y and Z directions, whereas a second-order accurate backward difference scheme was used to compute the vortex evolution in space (X) and time (T). Since both the U and W perturbations approach their limiting values at infinity (corresponding to equations 2.5d,e) rather slowly, the usage of higher order boundary conditions obtained through asymptotic considerations was found to be imperative in maintaining the spectral accuracy in the Y-direction. Overall, this numerical scheme combines a robust marching procedure with a strong coupling in the secondary-flow plane, the latter being especially desirable for solving vortex-flow problems. The accuracy of the numerical results was verified by grid-resolution checks, as well as through comparisons with analytical solutions, as discussed below.

3.1 Unsteady Evolution of Spanwise Periodic Perturbations

We will first discuss the results pertaining to the limit of the extra-long wavelength viscous vortices. We recall that this case has been considered by R. As pointed out in that paper, and as can be seen directly from the dispersion relation (2.9a), this regime admits a similarity behaviour of the type $X \sim Z^{6/5}$ and, $T \sim Z^{5/4}$, and hence, it is sufficient to consider the unsteady evolution of just a single Fourier mode in the spanwise direction; this we take to be $k = 1$ without any loss in generality. The real and imaginary parts of the spatial (β) root of this unsteady dispersion relation are shown in Fig. 3 for real values of the frequency $\omega(\equiv i\sigma)$. Unlike the case of cross-flow vortices, where the most unstable modes are usually time dependent, here the steady Görtler vortex ($\omega = 0$) is found to have the largest growth rate for any given spanwise wavenumber. This, along with the fact that a class of potentially dominant receptivity mechanisms preferentially excite the steady vortices as compared to unsteady ones (Choudhari and Streett, 1990), would help explain the observed dominance of steady Görtler vortices in laboratory experiments.

As shown in Fig. 3, the spatial growth rate decreases monotonically with frequency. A neutral point exists at $\omega = 2.298$ whilst in addition there is the asymptote $Re(\beta) \sim \frac{1}{\sqrt{2}}\frac{\omega}{d_2}^{3/2}$ as $\omega \to \infty$, with $d_2(\approx -3.2482)$ being the second zero of $Ai'(\zeta_0)$ on the negative real ζ_0 axis. On the other hand, the imaginary part of β is zero at $\omega = 0$, implying a purely exponential growth by the stationary vortex, as mentioned previously; but $Im(\beta)$ increases nearly monotonically as

ω is increased, leading to an asymptotic behaviour of $Im(\beta) \sim \frac{-1}{\sqrt{2}} \frac{\omega}{d_2}^{3/2}$ at large frequencies. One may also observe that, since the growth rate curve is locally stationary near its maximum at $\omega = 0$, the derivative $c_{gX} \equiv i\frac{d\omega}{d\beta}$, corresponding to the group velocity of the stationary vortices in the streamwise direction, is purely real and positive, equal to about 1.5 as seen from the dash-dot curve in Fig. 3. Of course, the behaviour of Görtler vortices is far from that of the mainly-oscillatory instability modes of the Tollmien-Schlichting or Rayleigh type, and hence, the notion of group velocity is not expected to be physically relevant in this case, especially for the $\omega = O(1)$ modes where the real and imaginary parts of c_{gX} are comparable to each other. Nevertheless, it is interesting to note that the real part of the group velocity in the X-direction is always positive, and less than its value for stationary vortices. Furthermore, the imaginary part of the group velocity is bounded for all spatial modes. Therefore, one might expect an impulsive source to generate a wavepacket with both ends propagating at finite speeds. This was indeed found to be the case in the numerical solutions, which are presented below.

For the purpose of simulating the transient wavepacket problem, we considered a hump shape of the form

$$F(X,Z,T) = (1 - cos(2\pi X))\ (1 - cos(4\pi T))\ cos(2\pi Z)\ R(X,0,1)R(T,0,0.5), \qquad (3.1a)$$

where $R(q,q_i,q_f)$ denotes the restriction operator in the q space, being equal to unity for $q_i < q < q_f$, and zero elsewhere. Similarly, in order to obtain the steady hump solution in a causal manner, an unsteady hump shape of the form

$$F(X,Z,T) = (1 - cos(2\pi X))\ (1 - e^{-T^2/4}))\ cos(2\pi Z)\ R(X,0,1), \qquad (3.1b)$$

was also considered.

For both these geometries, we have shown the behaviour of the displacement function $A(X,Z,T)$ along the vortex boundary $Z = 0$ as a function of X at selected instants of time in Figs. 4a and 4b respectively. Figure (4a) shows that the transient surface deformation generates a vortex patch downstream which increases in its streamwise extent, and in amplitude, with an increase in time. One may note that between $0 < X < 1$, the displacement function conforms quite closely to the hump-shape during the period $0 < T < 1$ when it is nonzero. Significantly the vortex pattern displays no oscillations in the streamwise direction at all. Thus, the boundary layer experiences a positive displacement at all times along the vortex boundary $Z = 0$, and a negative displacement along the centreline $Z = \pi$. As a result of the amplification with the passage of time, one would observe an increasingly stronger streaky structure corresponding to an alternate pattern of boundary layer upliftment (i.e. deceleration) and an equally strong attachment (i.e. acceleration) with a constant spacing along the streamwise direction. It will, of course, be very interesting to see how nonlinearity modifies this behaviour, and this will be the topic of a forthcoming paper. Finally, but most importantly, the convective nature of the spanwise periodic perturbations is seen very clearly from the downstream movement of the tail of the vortex patch; see, especially, the curves marked 12 through 15.

Figure 4b shows how the steady, spanwise-periodic vortex pattern gets established as the hump is brought to its final shape over a period of time. Again, one may note the monotonic behaviour of the displacement function $A(X, Z = 0, T)$ in the region downstream of the hump at each instant of time. In the vicinity of the hump, again, the displacement function closely resembles the instantaneous hump shape, as in the case of Fig. 4a. For small X, this latter

behaviour can also be predicted using the closed form solution (2.6) above, which further shows that for $X << 1$, the wall-shear perturbations $\bar{U}'(0)$ and $\bar{W}'(0)$ are considerably smaller than the displacement-thickness perturbation, being of $O(X^{4/3})$ and $O(X^{1/3})$, respectively, relative to $\bar{A}$. Furthermore, the viscous layer begins to grow at the usual rate of $Y \sim X^{1/3}$ near $X << 1$, thus suggesting a further split within the lower deck corresponding to $Y \sim X^{1/3}$ and $Y = O(1)$. The wall-shear scalings for small X show that the flow near the front end of the obstacle is nearly in the spanwise direction; however, contrary to what one's intuition might suggest, this flow is found to be converging towards the obstacle instead of spreading out along the spanwise direction. A physical explanation for this observation is provided in Section 3.2 below. The unstable, Görtler vortex part of the steady-state solution can be shown to be

$$A = \frac{3}{5}\beta_0 \bar{F}(\beta_0, k) e^{\beta_0 X}; \quad \beta_0 = (-3Ai'(0))^{3/5}, \tag{3.2}$$

which is shown via symbols in Fig. (4b). It may be seen that the numerical solution is in excellent agreement with the instability-mode part of it for nearly all locations downstream of the hump. Since the algebraically decaying part of the solution appears to be dominated so quickly by the unstable eigenfunction part, this suggests that experimental measurements of Görtler vortices need not only be carried out far downstream of the region where the vortices are induced.

Finally, let us briefly consider the inviscid limit corresponding to the dispersion relation (2.8a). It is easy to show that the corresponding differential equation for, say, the displacement function $\bar{A}$ is given by

$$\partial_X(\partial_X + |k|\partial_T)\bar{A} - k^2\bar{A} = 0, \tag{3.3}$$

which is hyperbolic in the $X - T$ space on the basis of the standard classification of second order partial differential equations. The two families of characteristic curves corresponding to equation (3.3) are given by

$$T = constant \quad \text{and} \quad X - |k|T = constant, \tag{3.4a,b}$$

respectively. This suggests that the Cauchy problem should be posed at some initial station $X = 0$, and if the Cauchy data has a finite nonzero limit as $T \to \infty$, one duly obtains the unstable Görtler vortex growing in the downstream direction as part of the causal steady solution. In contrast, if one traces the trajectories of both roots of the dispersion relation (2.8a) in the complex β plane as σ moves from positive infinity to zero along the real axis (Fig. 5), then application of the Briggs-Bers criterion would imply that the root corresponding to the unstable vortex ought to appear on the upstream side. The reason behind this failure appears to be linked to the infinite-speed characteristic (3.4a), which leads to a solution that does not decay rapidly enough in X at any instant of time, thereby disallowing the usage of the imaginary β axis as the inversion contour for a two-sided Laplace transform in X even for small values of T. Since the Briggs-Bers criterion is based on the assumption of a spatially compact disturbance at small enough times, it seems reasonable to expect that that it may not provide reliable results in this particular case. This peculiar behaviour of the instability in question is also reflected in the dispersion relation (2.8a), which predicts purely dispersive behaviour for real streamwise wavenumbers (i.e. neutral behaviour in the sense of a temporal instability), but predicts unstable roots for real frequencies (i.e. spatial instability), in particular, the stationary Görtler vortex at $\omega = 0$.

3.2 Unsteady and Steady Disturbance Patterns due to Localized Surface Irregularities

In view of the order of magnitude increase in the computational effort required for this case, only one specific situation, corresponding to

$$F(X,Z,T) = (1 - cos(2\pi X))\,(1 - cos(4\pi T))\,e^{-Z^2/9}\,R(X,0,1)\,R(T,0,0.5), \qquad (3.5)$$

was considered for the purpose of numerically calculating the disturbance pattern due to an unsteady, localized wall hump. Here, the Gaussian drop-off in the spanwise spectrum was chosen in order to offset the ill-posedness of the steady dispersion relationship (2.9b). The contours of constant (instantaneous) displacement in the $X-Z$ plane for this case have been shown for a few selected values of time in Figs. (6a-e). Due to the spanwise symmetry of the surface obstacle, only positive values of the spanwise coordinate Z have been included in the plot. Results for negative values of Z can be obtained through a reflection of the contour about the horizontal (X) axis. Figures 6a-e clearly indicate that a vortex pattern is established downstream of the source, and that as time passes, this pattern is convected downstream, also gaining in amplitude at the same time. This further demonstrates the convective nature of Görtler instability in the case of disturbances with a continuous spectrum of spanwise wavenumbers. Thus, it would be possible to study the disturbances produced by a steady wall hump by a direct solution of the steady form of the governing equations.

For the purpose of the steady calculation, we considered the hump shape given by

$$F(X,Z) = (1 - cos(2\pi X))\,e^{-Z^2/9}\,R(X,0,1). \qquad (3.6)$$

The constant displacement contours corresponding to the disturbance pattern produced by this hump are shown in Fig. 7a. One may observe that the confocal ellipses near the inflow boundary conform rather closely with the obstacle shape, similar to that in the spanwise-periodic case discussed in Section 3.1 above. Thus, over a major part of the hump, the boundary layer is simply lifted up by the amount of the local obstacle height, although in the downward sloping portion of the hump, there are regions of small negative displacement at sufficiently large values of the spanwise coordinate Z. Figure 7a also indicates the presence of a streamwise corridor just downstream of the hump (corresponding to curve 6 closest to the X-axis), which separates the region of large (positive) displacement from the relatively less disturbed region outside. This feature was also noted by Smith *et al* (1977) in the solution to a three-dimensional triple deck problem. The most striking feature in Fig. 7a, however, is the gradual emergence of a vortex structure downstream of the hump, which corresponds to alternating regions of positive and negative displacement, separated by the contours marked as "6". At each streamwise station, the innermost vortex is the strongest one, with the amplitude falling off rather rapidly away from the centreline, thus leading to a vortex pattern with a roughly parabolic shape. The orientations of the centrelines of different vortices, corresponding to zero displacement contours (marked as "6" in the figure), indicate that all of the vortices are present at locations just downstream of the hump; however, since their amplitudes are inversely proportional to the distance away from the axis ($Z = 0$), the more distant vortices become noticeably large only at increasingly larger distances, thereby creating the illusion that additional vortices are being created as one moves downstream. The qualitative resemblance between the vortex patch of

Fig. (7a) and that computed numerically for the case of $G = O(1)$ and $\lambda_z = O(1)$, Denier, Hall and Seddougui (1990), where no asymptotic approximations were involved, indicates that the presence of spanwise diffusion terms in the governing equations is not a prerequisite to obtain a slowly spreading pattern of streamwise vortices.

The contours of constant axial and spanwise shear stresses (not shown here) also bear some similarities to the triple deck situation, excepting the lack of upstream influence, and the presence of the Görtler vortex pattern. However, an examination of the secondary flow within the $X - Z$ plane reveals an important difference between the disturbance patterns in these two cases. Specifically, the results of Smith *et al* (1977) show that on the forward face of the hump, the fluid is pushed out in the spanwise direction within the lower deck, although it converges again towards the obstacle inside the middle deck, thus creating a recirculating secondary-flow pattern. This pattern is reversed on the backward face of the hump, whereby the fluid is drawn together in the lower deck, but pushed out within the middle-deck. Contrary to this, as well as to one's intuitive expectations, it is found that in the case of an obstacle over a concave surface, the fluid moves towards the obstacle on both the forward, as well as rear faces of the hump. This spanwise convergence of the fluid, which continues across the middle deck as well, is accompanied by an upwelling near the axis ($Z = 0$), thereby setting up an outflux into the upper deck, where the fluid is pushed out again; see Fig. (7b). The counterrotating vortices generated in this manner become especially prominent farther downstream of the obstacle, and one observes the distinct pattern of alternate regions of upwelling and downwelling, with the strength of this pattern decreasing quite rapidly away from the axis.

These differences between the two problems can be easily traced to the nature of the respective relationships between the pressure and the displacement-thickness perturbations. In the case of an obstacle with triple-deck scalings over a flat surface, the distribution of pressure is controlled by the streamwise slope of the displacement function, whereas in the case of a streamwise elongated hump over a concave wall, the pressure is equal to the negative of the displacement, as seen from the viscous limit of the interactive relationship (2.3f). Therefore, the decreasing displacement away from the centreline in Fig. 7a translates into a negative pressure perturbation of decreasing magnitude away from the axis, $Z = 0$. In other words, the displacement pattern of Fig. 7a induces a favorable pressure gradient towards the centreline, which would explain the sink-like effect the obstacle has on the flow within the boundary layer.

4 Conclusions

We have investigated the unsteady spatial evolution of long wavelength Görtler vortices in a boundary layer. The viscous-inviscid interactive regime we have considered is appropriate to situations when the Görtler number is large but any perturbations in the flow have spanwise wavelength much larger than the boundary layer thickness. In particular it follows that our work is relevant to flows near the leading edge of highly curved boundary layers of the type one might find for example on a turbine blade.

We have shown that the Görtler mechanism in this regime is a convective rather than absolute instability. This result contradicts previous work on the Görtler problem in this part of the Görtler-wavenumber space. Perhaps the main conclusion to be drawn from our work is that in general it is sufficient to study only the steady Görtler problem. However we must bear in

mind that our analysis is restricted to the small wavenumber regime so that it is always possible that absolute instabilities might occur at larger wavenumbers. The fact, that experimental observations all indicate that Görtler vortices are convectively unstable, suggests that the latter scenario is unlikely.

Acknowledgements

One of us (MC) would like to acknowledge the financial support by the Theoretical Flow Physics Branch of the NASA Langley Research Center, under Grant No. NAS-18240. The research of PH was carried out while he was in residence at ICASE, NASA Langley Research Center. The authors would like to thank Prof. O. S. Ryzhov for pointing out related work by Ruban and colleagues. The authors also thank Dr. Ruban for discussions concerning his work, and Prof. D. T. Papageorgiou for his comments. MC also thanks Dr. M. Y. Hussaini for his encouragement.

References

Balsa, T. F. 1988 On the receptivity of free shear layers to two-dimensional external excitation. *J. Fluid Mech.*, **187**, pp. 155-177.

Bers, A. 1975 Linear Waves and Instabilities,In Physique des Plasmas. ed. C. DeWitt, J. Peyraud, pp. 117-215, New York, Gordon and Breach

Briggs, R. J. 1964 Electron-Stream Interactions with Plasmas. Cambridge, Mass.: MIT Press.

Choudhari, M., and Streett, C.L., 1990 Boundary Layer Receptivity Phenomena in Three-Dimensional and High-Speed Boundary Layers,*AIAA Paper 90-5258.*

Denier, J. P., Hall, P. and Seddougui, S. O. 1990 On the receptivity problem for Görtler vortices: vortex motions induced by wall roughness. *ICASE Report*, **90-31.** Also appeared as *Phil. Trans. R. Soc. Lond. A.*, **335**, 51–85.

Hall, P. 1982*a* Taylor–Görtler vortices in fully developed or boundary layer flows: linear theory. *J. Fluid Mech.*, **124**, 475–494.

Hall, P. 1982*b* On the nonlinear evolution of Görtler vortices in growing boundary layers. *J. Inst. Maths. and Applications*, **29**, 173.

Hall, P. 1983 The linear development of Görtler vortices in growing boundary layers. *J. Fluid Mech.;* **130**, 41–58.

Hall, P. 1988 The nonlinear development of Görtler vortices in growing boundary layers. *J. Fluid Mech.*, **193**, 247–266.

Hall, P. 1990 Görtler vortices in growing boundary layers: the leading edge receptivity problem, linear growth and the nonlinear breakdown stage. *Mathematika*, **37**, 151-189.

Hall, P. and Lakin, W. D. 1988 The fully nonlinear development of Görtler vortices in growing boundary layers. *Proc. R. Soc. Lond. A*, **415**, 421–444.

Hall, P. and Morris, H. 1991 On the instability of heated boundary layers on flat plates.*ICASE Report*, **91-44**. . Also to appear in *J. Fluid Mech.*.

Huerre, P. and Monkewitz, P. A. 1985 Absolute and Convective I nstabilities in Free Shear Layers. *J. Fluid Mech.* **159**, 159–168.

Liu, J. T. C. and Sabry, A. S., 1991 Concentration and heat transfer in nonlinear Görtler vortex flow and the analogy with longitudinal momentum transfer. *Proc. Roy. Soc. LOndon Ser. A* **432**, p. 1.

Parks, D. and Huerre, P. 1988 On the Convective Nature of the Gör tler Instability,*Bull. Am. Phys. Soc.*. **33**, p. 2252.

Rozhko, S. B., and Ruban, A. I., 1987 Longitudinal-Transverse Interaction in a Three-Dimensional Boundary Layer. *Mekh. Zidk. Gaza*, **3**, 42–.

Rozhko, S. B., Ruban, A. I., and Timoshin, S. N., 1988 Interaction of a Three-Dimensional Boundary Layer with an Extensive Obstacle.*Mekh. Zidk. Gaza*, **1**, 39-48.

Ruban, A. I. 1990 Propagation of wave packets in the boundary layer on a curved surface. *Izv. Akad. Nauk. SSSR., Mekh. Zhidk. Gaza.*,**2**, 59-68.

Sabry, A. S. and Liu, J. T. C., 1991 Longitudinal Vorticity Elements in Boundary Layers: Their nonlinear development from initial Görtler vortices as a prototype problem.*Brown University Division of Engineering Research Report No. FM89-11, 1989*; also *J. Fluid Mech.* **231**, p. 615, 1991.

Savenkov, I. V., 1990 Instability of the Boundary Layer on a Curved Surface.*Mekh. Zidk. Gaza*, **1**, 176–179.

Smith, F. T., Sykes, R. I. and Brighton, P. W. M., 1977 A two-dimensional boundary layer encountering a three-dimensional hump. *J. Fluid Mech.*, **83**, 163–176.
Timoshin,S. N. 1990 Asymptotic Analysis of a Spatially Unstable Görtler Vortex Spectrum.*Mekh. Zidk. Gaza*, **1**, 32–41.

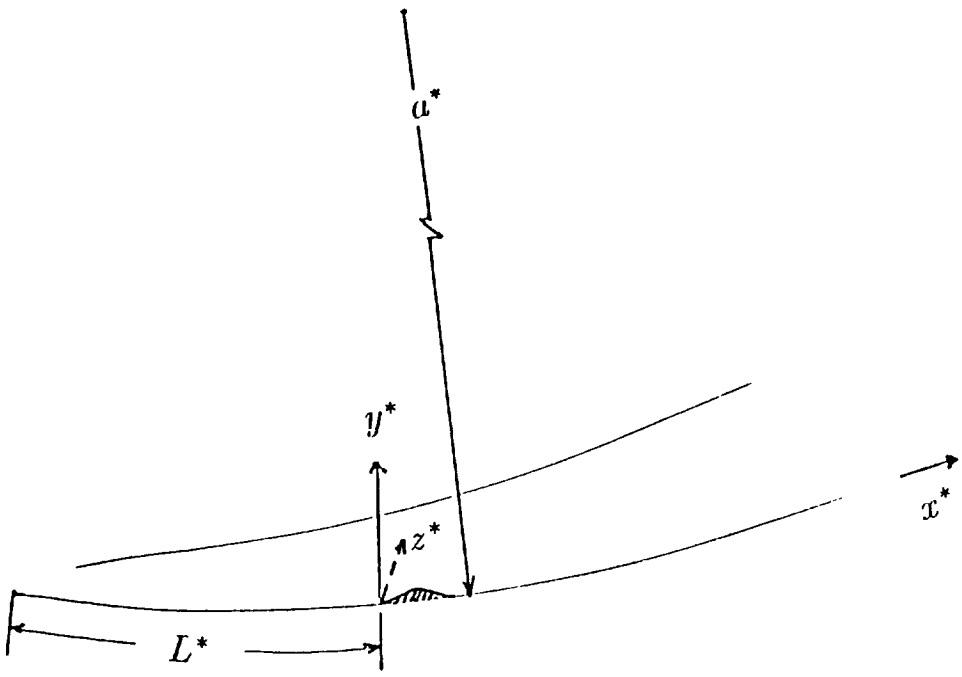

Fig. 1 Schematic of the problem.

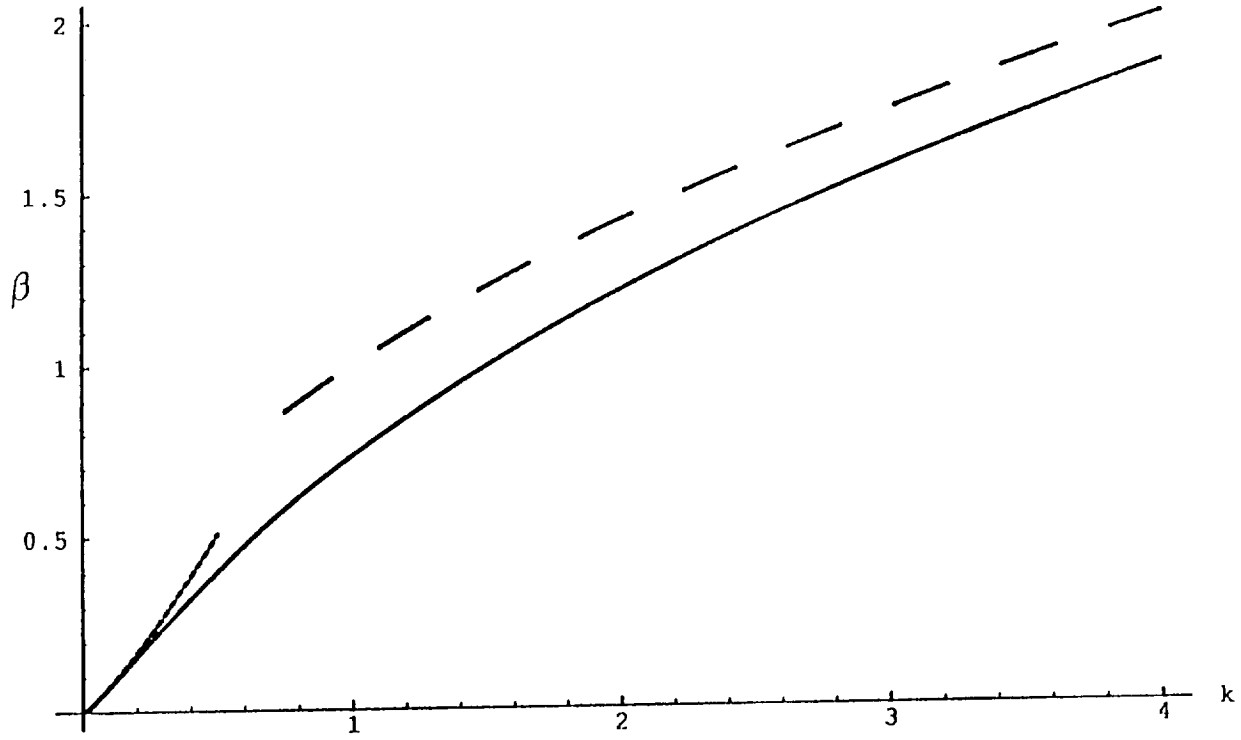

Fig. 2 Spatial root of the steady dispersion relation (2.7b)

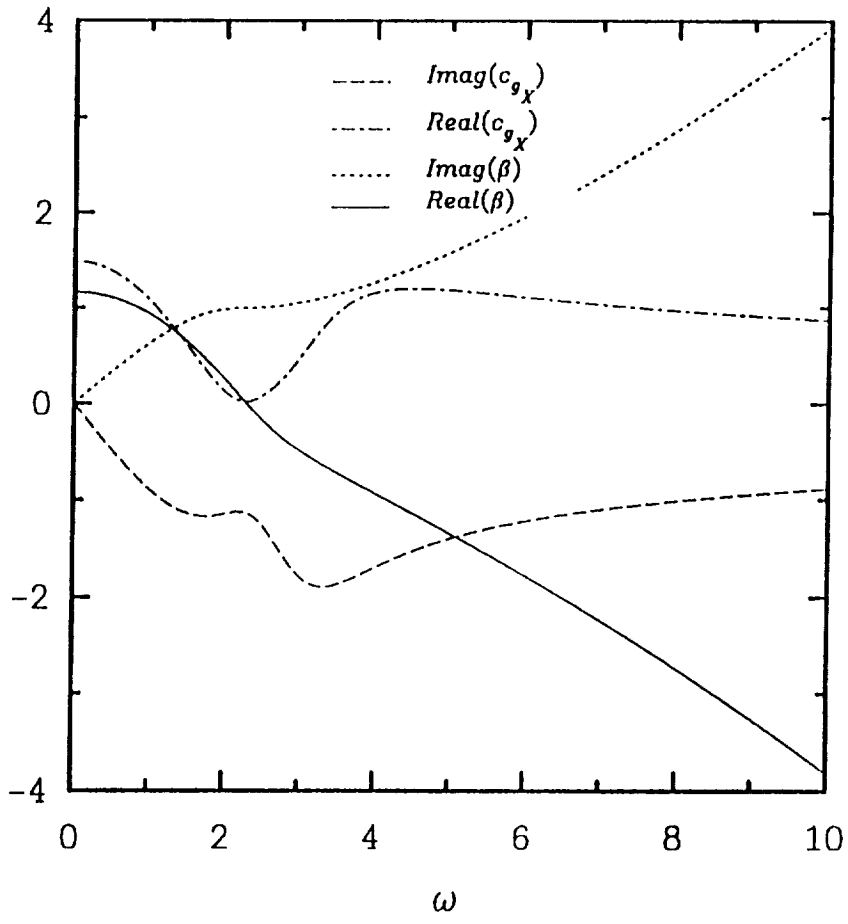

Fig. 3 Spatial instability properties of the unsteady dispersion relation (2.9a) for $k = 1.0$.

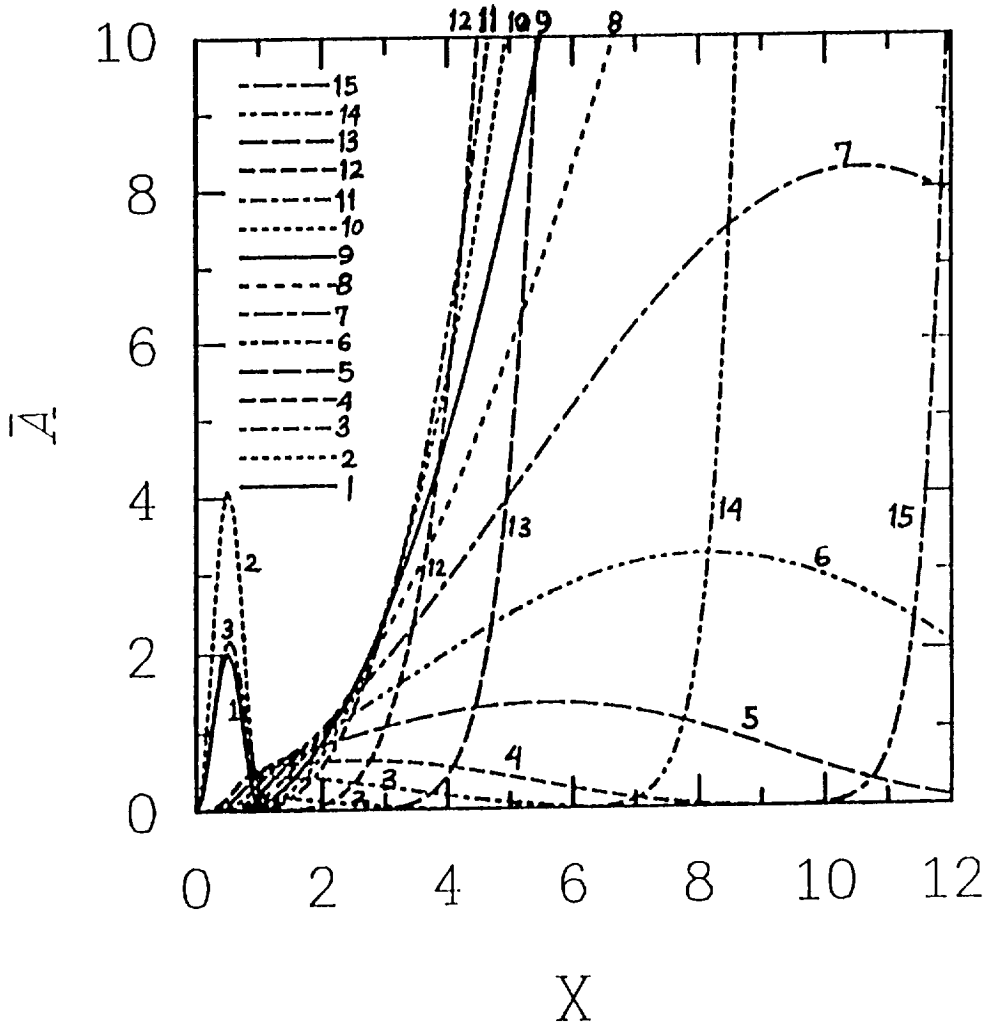

Fig. 4 Displacement function $A(X, Z, T)$ along the vortex boundary $Z = 0$ as a function of X at selected values of time

(a) $F(X, Z, T) = (1-cos(2\pi X))\ (1-cos(4\pi T))\ cos(2\pi Z)\ R(X, 0, 1)R(T, 0, 0.5)$
Curves 1 through 15 correspond to T=0.125, 0.250, 0.375, 0.5, 0.75, 1.0, 1.25, 1.5, 1.75, 2.0, 2.25, 3.5, 6.0, 12.25, and 18.5, respectively.

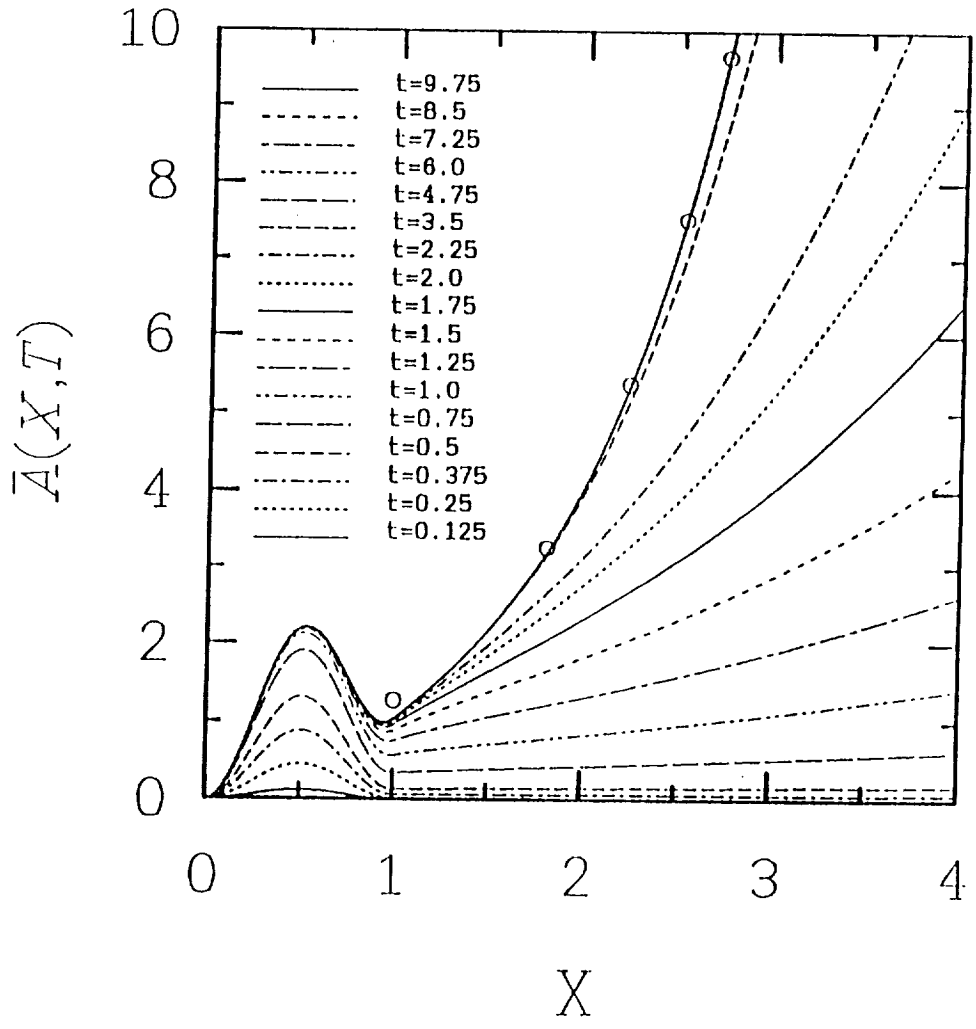

Fig. 4 Displacement function $A(X, Z, T)$ along the vortex boundary $Z = 0$ as a function of X at selected values of time

(b) $F(X, Z, T) = (1 - cos(2\pi X))\,(1 - e^{-T^2/4}))\,cos(2\pi Z)\;R(X, 0, 1)$

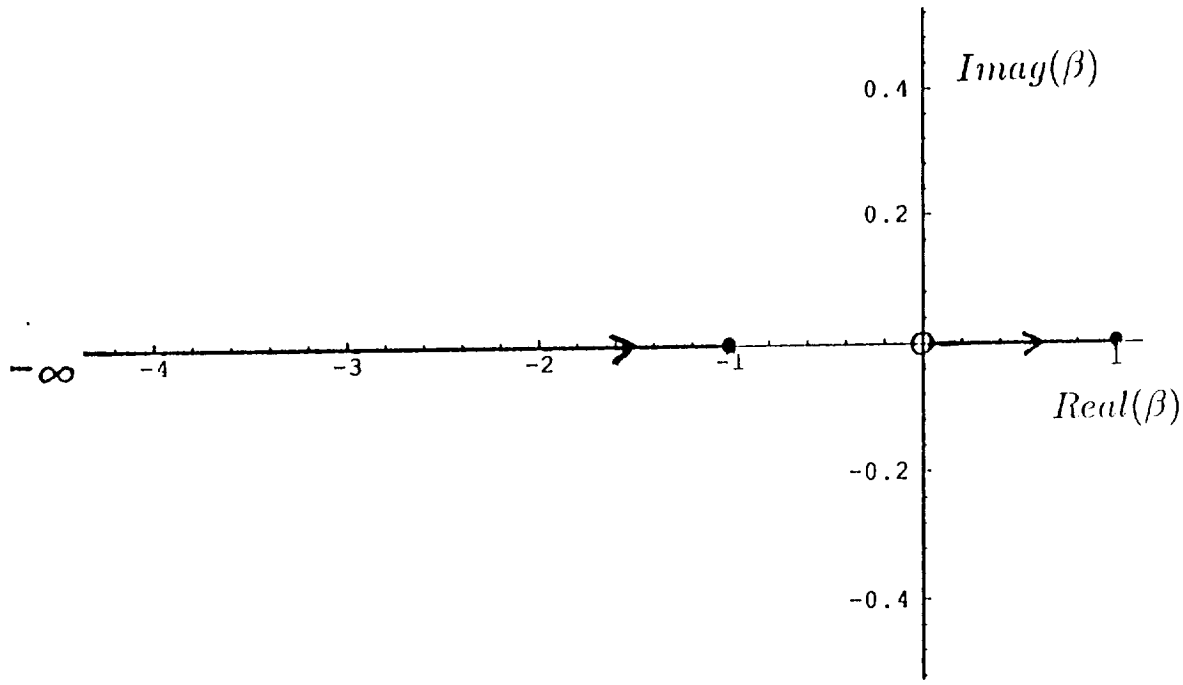

Fig. 5 Trajectories of the spatial roots of the inviscid dispersion relation (2.8a) in the complex β plane as σ moves from $+\infty$ to 0 along the real axis

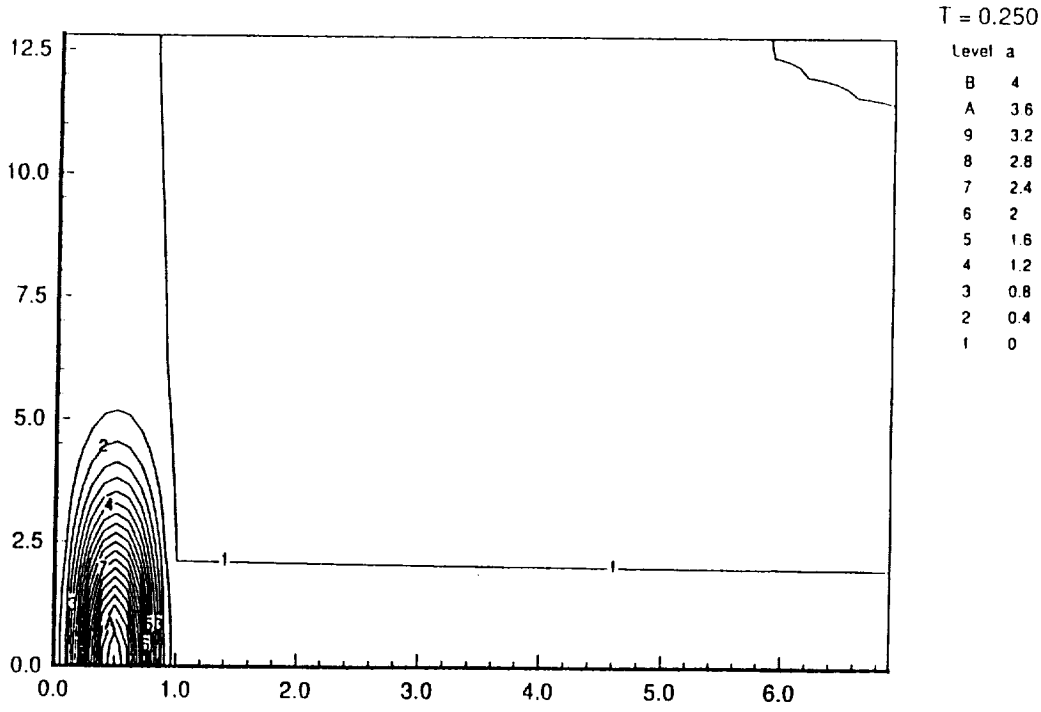

(a) $T = 0.250$

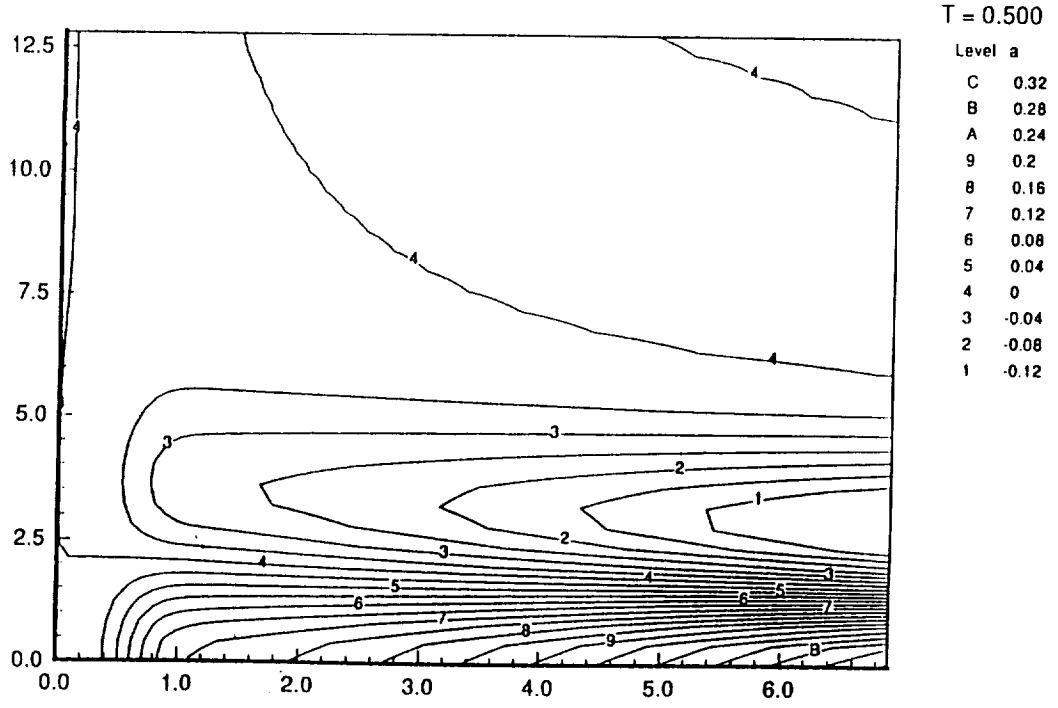

(b) $T = 0.500$

Fig. 6 Contours of constant displacement perturbation at selected instants of time for hump shape corresponding to equation (3.5)

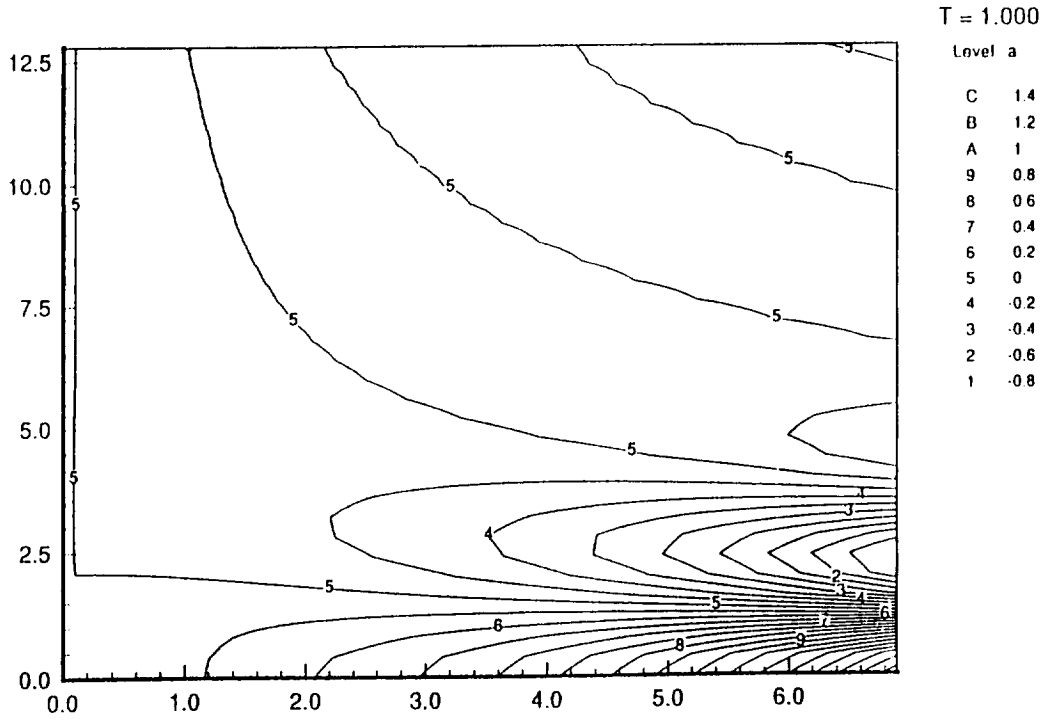

(c) $T = 1.000$

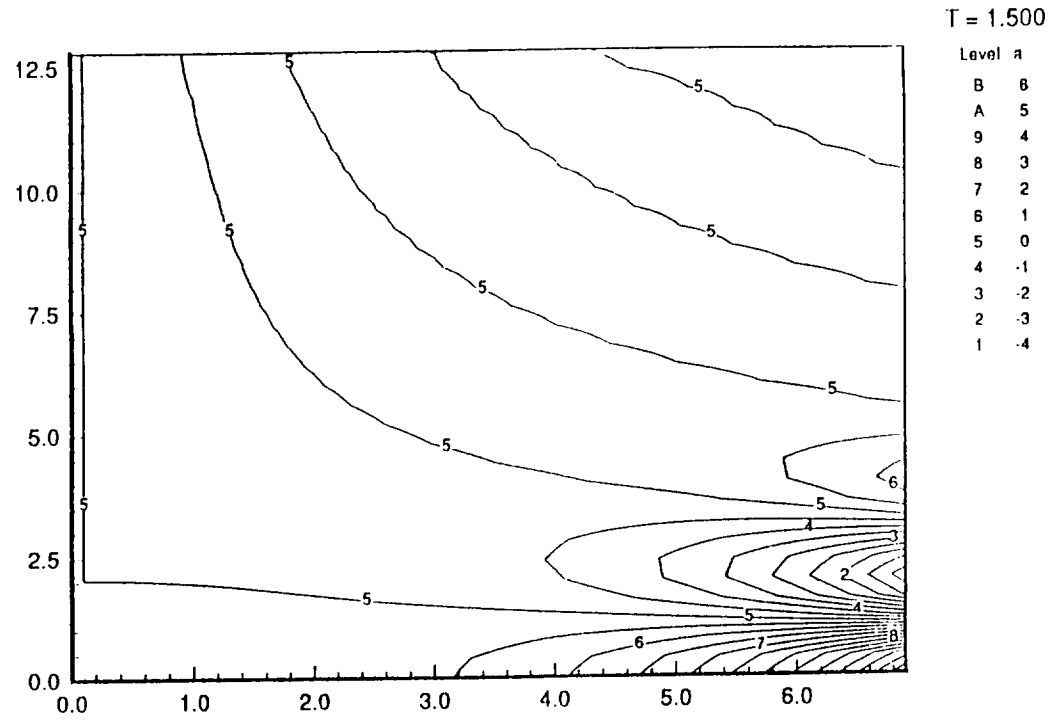

(d) $T = 1.500$

Fig. 6

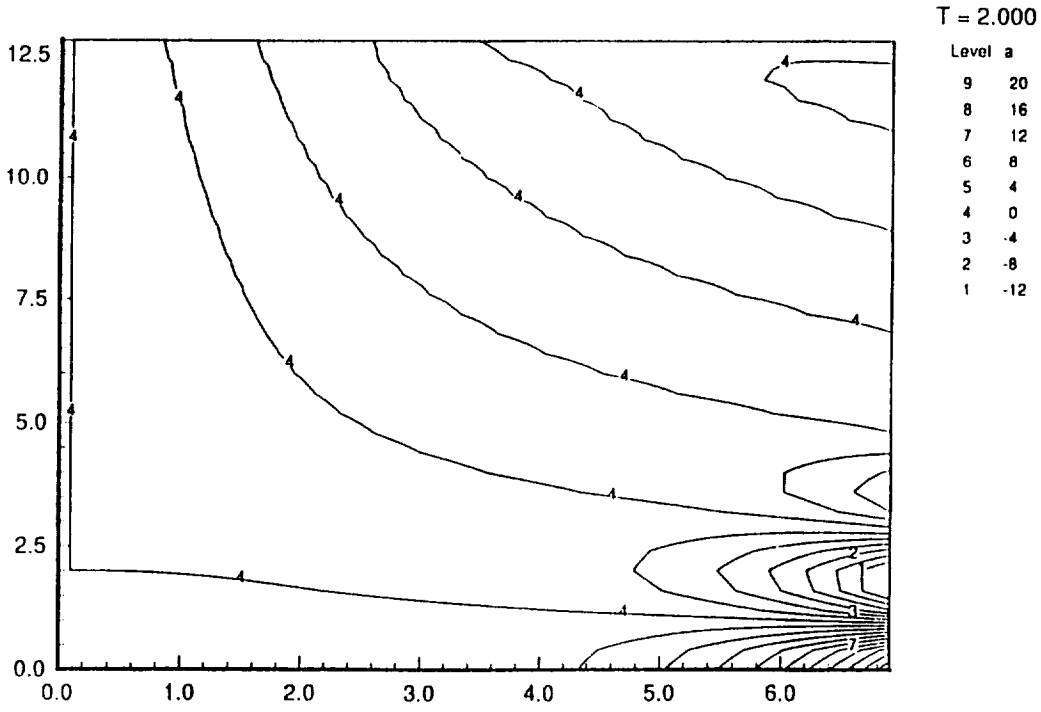
T = 2.000
Level a
9 20
8 16
7 12
6 8
5 4
4 0
3 -4
2 -8
1 -12
12.5
10.0
7.5
5.0
2.5
0.0
0.0
1.0
2.0
3.0
4.0
5.0
6.0

(e) $T = 2.000$

Fig. 6

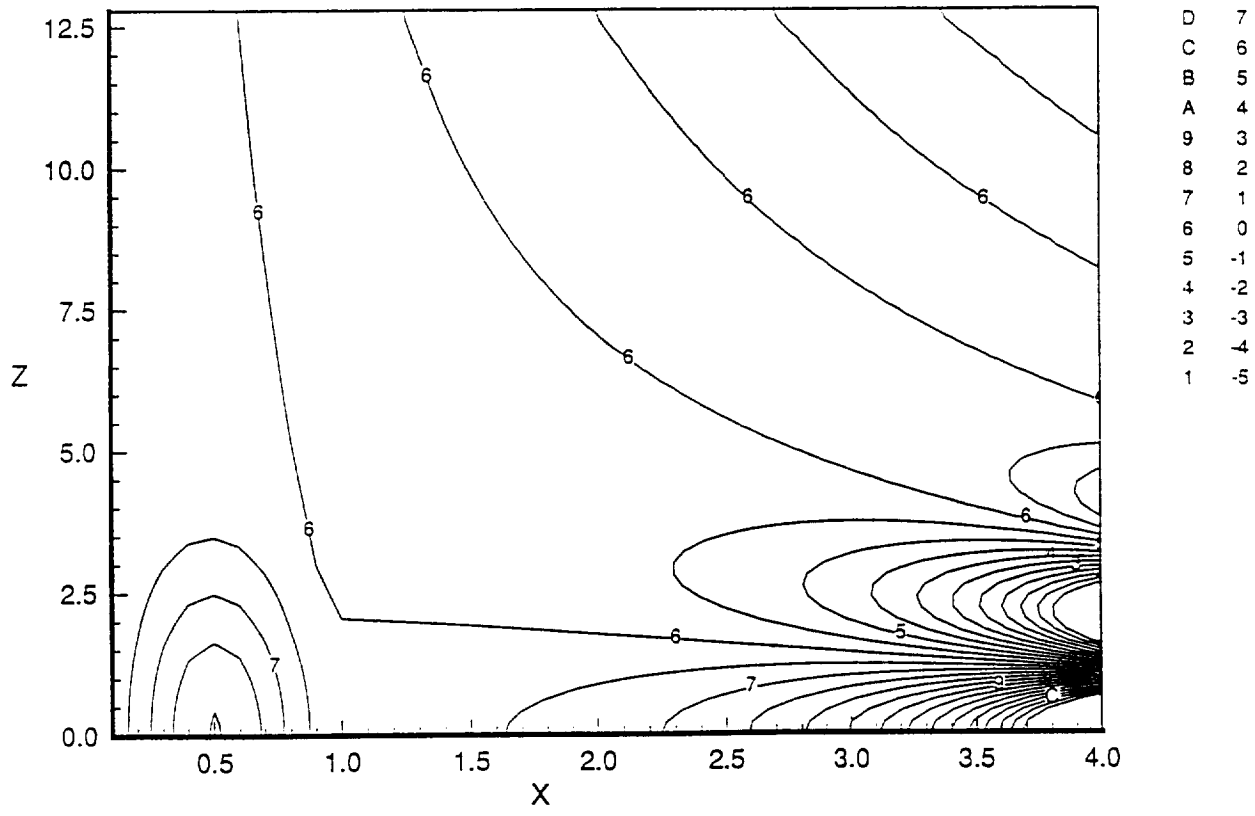

Fig. 7a Contours of constant displacement perturbation for the steady hump (3.6)

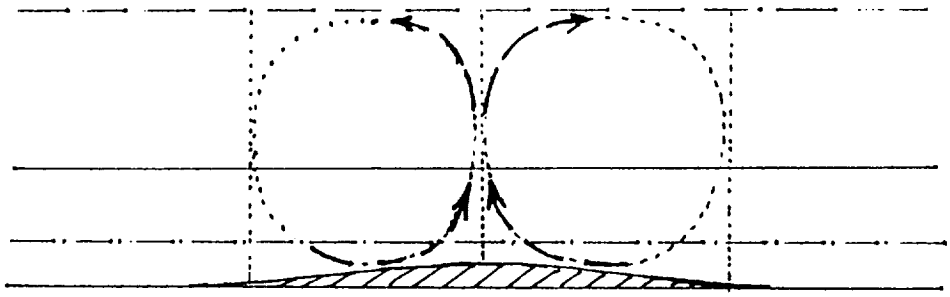

Fig. 7b Sketch of the secondary-flow pattern due to a wall hump on a concave surface

REPORT DOCUMENTATION PAGE

Form Approved
OMB No. 0704-0188

1. AGENCY USE ONLY (Leave blank)	2. REPORT DATE	3. REPORT TYPE AND DATES COVERED
	July 1992	Contractor Report

4. TITLE AND SUBTITLE
ON THE SPATIAL EVOLUTION OF LONG-WAVELENGTH GÖRTLER VORTICES GOVERNED BY A VISCOUS-INVISCID INTERACTION
PART 1: THE LINEAR CASE

5. FUNDING NUMBERS
C NAS1-18605
WU 505-90-52-01

6. AUTHOR(S)
Meelan Choudhari
Philip Hall
Craig Streett

7. PERFORMING ORGANIZATION NAME(S) AND ADDRESS(ES)
Institute for Computer Applications in Science and Engineering
Mail Stop 132C, NASA Langley Research Center
Hampton, VA 23665-5225

8. PERFORMING ORGANIZATION REPORT NUMBER
ICASE Report No. 92-31

9. SPONSORING/MONITORING AGENCY NAME(S) AND ADDRESS(ES)
National Aeronautics and Space Administration
Langley Research Center
Hampton, VA 23665-5225

10. SPONSORING/MONITORING AGENCY REPORT NUMBER
NASA CR-189681
ICASE Report No. 92-31

11. SUPPLEMENTARY NOTES
Langley Technical Monitor: Michael F. Card
Final Report

Submitted to
Q.J.M.A.M.

12a. DISTRIBUTION/AVAILABILITY STATEMENT
Unclassified - Unlimited

Subject Category 34

12b. DISTRIBUTION CODE

13. ABSTRACT *(Maximum 200 words)*

The generation of long-wavelength, viscous-inviscid interactive Görtler vortices is studied in the linear regime by numerically solving the time-dependent governing equations. It is found that time dependent surface deformations, which assume a fixed nonzero shape at large times, generate steady Görtler vortices that amplify in the downstream direction. Thus, the Görtler instability in this regime is shown to be convective in nature, contrary to the earlier findings of Ruban and Savenkov. The disturbance pattern created by steady and streamwise-elongated surface obstacles on a concave surface is examined in detail, and also contrasted with the flow pattern due to roughness elements with aspect ratio of order unity on flat surfaces. Finally, the applicability of the Briggs-Bers criterion to unstable physical systems of this type is questioned by providing a counterexample in the form of the inviscid limit of interactive Görtler vortices.

14. SUBJECT TERMS
vortices; viscous-inviscid interaction

15. NUMBER OF PAGES
28

16. PRICE CODE
A03

17. SECURITY CLASSIFICATION OF REPORT	18. SECURITY CLASSIFICATION OF THIS PAGE	19. SECURITY CLASSIFICATION OF ABSTRACT	20. LIMITATION OF ABSTRACT
Unclassified	Unclassified		

NSN 7540-01-280-5500

Standard Form 298 (Rev 2-89)
Prescribed by ANSI Std Z39-18
298-102

NASA-Langley, 1992